Journal of
Synchrotron Radiation

ISSN 0909-0495

Received 22 September 2009
Accepted 15 July 2010

A variable-wavelength-based approach of phase retrieval for contrast transfer function based methods

Yogesh S. Kashyap,* Ashish Agrawal, P. S. Sarkar, Mayank Shukla, Tushar Roy and Amar Sinha

Laser and Neutron Physics Division, Bhabha Atomic Research Centre, Trombay, Mumbai-40085, India. E-mail: yogesh78@barc.gov.in

X-ray phase-contrast imaging has emerged as an important method for improving contrast and sensitivity in the field of X-ray imaging. This increase in the sensitivity is attributed to the fact that, in the hard X-ray regime, the phase shift is more prominent as compared with the attenuation for materials having a low X-ray absorption coefficient. Among all the methods using the X-ray phase-contrast technique, in-line phase-contrast imaging scores over the other methods in terms of ease of implementation and efficient use of available X-ray flux. In order to retrieve the projected phase map of the object from the recorded intensity pattern, a large number of algorithms have been proposed. These algorithms generally use either the transport of intensity or contrast transfer function based approach for phase retrieval. In this paper it is proposed to use multiple wavelengths for phase retrieval using the contrast transfer function based formalism.

Keywords: X-ray imaging; phase contrast; phase retrieval.

1. Introduction

The conventional absorption-based X-ray imaging techniques suffer from the drawback of low sensitivity to small density variations and low X-ray absorption contrast for materials such as polymers, foam and carbon composites. X-ray phase-contrast imaging has emerged as a new tool in probing such kinds of materials. These techniques can offer up to a 1000-fold increase in sensitivity with hard X-rays. A large number of techniques and methods have been developed to obtain the phase contrast (Wilkins *et al.*, 1996; Momose, 2003; Bonse & Hart, 1965; Chapman *et al.*, 1997; David *et al.*, 2002; Snigirev *et al.*, 1995; Pfeiffer *et al.*, 2006; Cloetens *et al.*, 1996) using hard X-rays. Among these the propagation-based technique offers a unique advantage in terms of its simplicity and ease of implementation. In this method, phase contrast is achieved by allowing a spatially coherent X-ray beam to propagate a sufficient distance in free space after the object. The contrast in the recorded image depends upon parameters such as X-ray wavelength, propagation distance, complex refractive index, *etc.* The transport-of-intensity equation shows (Teague, 1982, 1983) that variables, namely the phase shift induced by the sample, the contrast recorded at the detector and the sample-to-detector distance D, are related by a simple differential equation. This equation can be easily solved using suitable boundary conditions to retrieve the projected phase map or refractive index of the material (Nugent *et al.*, 1996; Gureyev & Nugent, 1997; Barty *et al.*, 1998; Paganin & Nugent, 1998). This technique in turn can be coupled with conventional tomography methods to find the full volume or the three-dimensional distribution of refractive index of the material (Bronnikov, 2002; Groso *et al.*, 2006). More complicated phase-retrieval algorithms to facilitate accurate retrieval of the phase have also been proposed (Gureyev, Pogany *et al.*, 2004; Meng *et al.*, 2007; Allen & Oxley, 2001). These algorithms relax some of the constraints of the transport-of-intensity equation and tend to be more stable, and are valid for a large class of samples and large propagation distances. In this paper we investigate the use of a multi-wavelength-based phase-retrieval approach for quantitative phase retrieval. The motivation for the present work comes from an earlier proposed multi-wavelength approach to retrieve the phase distribution using the transport of intensity equation (Gureyev *et al.*, 2001). The robustness of this method has already been demonstrated within the framework of the transport-of-intensity equation (Gureyev *et al.*, 2002; Gureyev, Paganin *et al.*, 2004). We propose to investigate this approach to retrieve the projected phase map for contrast transfer function (CTF)-based methods. The multi-wavelength approach seems to be more attractive for retrieving the phase map for CTF-based phase-retrieval methods as compared with the transport-of-intensity approach. The major reason for this is that in the transport-of-intensity approach, in order to retrieve the phase, one needs to collect data at two different object-to-detector

distances. However, the projected phase map of the object in CTF-based methods is retrieved by collecting data at different object-to-detector distances and then processing the data using suitable algorithms. This approach is akin to least-squares minimization with respect to distances. The change in object position results in the misalignment of the acquired images (linear and angular) and hence one has to again align all the data before actual computation. Thus it not only increases the computational complexity but also decreases the efficiency of the CTF-based phase-retrieval techniques. The complexity of this approach increases if one has to obtain a full three-dimensional distribution of the refractive index of the object (Cloetens *et al.*, 1999). In this case such a process has to be repeated for every angle for which the data have been collected. In contrast to the variable-distance approach, the multi-wavelength approach does not involve any motion of the sample or detector. Moreover, the change in wavelength can be made more precisely and easily owing to the availability of high-quality X-ray monochromators. Thus by using the multi-wavelength approach the requirement of motion of detector or sample and associated problems such as misalignment of images is obviated. This would not only decrease data collection time but also reduce the complexity of the retrieval process.

In this paper we demonstrate the suitability of this approach for phase retrieval of weakly absorbing material using simulated and experimental data.

2. Method of the CTF-based phase-retrieval approach

Let us consider an object with complex refractive index $n(\mathbf{r}, \lambda) = 1 - \delta(\mathbf{r}, \lambda) - i\beta(\mathbf{r}, \lambda)$ where $\mathbf{r} = (\mathbf{x}, z)$, $\mathbf{x} = (x, y)$. Let this be illuminated with coherent X-rays of wavelength λ. The weak interaction of X-rays with the object allows us to neglect the diffraction effects within the object, and its transmission function can be modeled as

$$T(\mathbf{x}) = a(\mathbf{x}) \exp[i\varphi(\mathbf{x})] = \exp[M + i\varphi(\mathbf{x})]$$

where $M = -(2\pi/\lambda) \int \beta(\mathbf{x}, z', \lambda)\, \mathrm{d}z'$ is the attenuation and $\varphi = -(2\pi/\lambda) \int \delta(\mathbf{x}, z', \lambda)\, \mathrm{d}z'$ represents the phase shift.

In the in-line phase-contrast imaging, the contrast is obtained due to the free-space propagation of the beam which transforms phase variations in the object plane into detectable intensity variations in the image plane. Depending upon the distance between the detector and the object, one can classify the region as the near-field region and far-field region. In the near-field region the recorded pattern is very similar to the exit wavefield convolved with the free-space propagator or the Fresnel propagator $(1/i\lambda z) \exp[i(\pi/\lambda z)|\mathbf{x}'|^2)]$. Mathematically the intensity at the distance z from the object plane is described by the following equation,

$$I_z = \left| T(\mathbf{x}') * (1/i\lambda z) \exp\left[i(\pi/\lambda z) \left| \mathbf{x}' \right|^2 \right] \right|^2. \quad (1)$$

The Fourier transform of the intensity pattern in the detector plane can be expressed as [(Guigay, 1977)]

$$\tilde{I}_z(\mathbf{f}) = \int T\left(\mathbf{x} - \frac{\lambda z \mathbf{f}}{2}\right) T^*\left(\mathbf{x} + \frac{\lambda z \mathbf{f}}{2}\right) \exp(-i2\pi \mathbf{x} \cdot \mathbf{f})\, \mathrm{d}\mathbf{x}, \quad (2)$$

where $\mathbf{f} = (f_x, f_y)$ are the spatial frequency co-ordinates, $\mathbf{x} \cdot \mathbf{f}$ denotes the scalar product, and z is the distance between the object and detector.

Under the assumption of weak absorption and slowly varying phase [$M(x) \ll 1$ and $|\varphi(\mathbf{x} + \lambda z \mathbf{f}) - \varphi(\mathbf{x} - \lambda z \mathbf{f})| \ll 1$], equation (2) can be simplified to (Turner *et al.*, 2004; Zabler *et al.*, 2005; Guigay *et al.*, 2007)

$$\tilde{I}(\mathbf{f}) = \tilde{\delta}(\mathbf{f}) + 2\sin(\pi\lambda z |\mathbf{f}|^2)\tilde{\varphi}(\mathbf{f}) - 2\cos(\pi\lambda z |\mathbf{f}|^2) \frac{\lambda z}{2\pi} \tilde{M}(\mathbf{f}), \quad (3)$$

where $\tilde{\varphi}$ represents the Fourier transform of the bracketed quantity φ, $\tilde{M}$ represents the Fourier transform of the absorption, and $\tilde{I}_z(\mathbf{f})$ is the Fourier transform of the intensity at distance z. This equation can be solved in the sense of least-squares minimization by collecting the data at various distances using the following equation (Langer *et al.*, 2008),

$$\tilde{\varphi}(\mathbf{f}) = \frac{1}{2(BC - A^2)} \Big[C \sum_z \tilde{I}_z(\mathbf{f}) \sin(\pi\lambda z |\mathbf{f}|^2) - A \sum_z \tilde{I}_z(\mathbf{f}) \cos(\pi\lambda z |\mathbf{f}|^2) \Big] \quad (4)$$

where

$$A = \sum_z \sin(\pi\lambda z |\mathbf{f}|^2) \cos(\pi\lambda z |\mathbf{f}|^2),$$
$$B = \sum_z \sin^2(\pi\lambda z |\mathbf{f}|^2,$$
$$C = \sum_z \cos^2(\pi\lambda z |\mathbf{f}|^2).$$

3. Multi-energy approach for the weak absorption case

The solution of equation (3) was achieved by collecting data at different distances and then processing the data. In order to derive the formulation based on the multiple-wavelength approach, we make a few approximations. It is assumed that the data are collected away from the absorption edge of any material that may be present in a given material. The dependencies of the real and imaginary parts of the complex refractive index on the wavelength of the incident radiation in the absence of absorption edges between λ and λ' for any elements present in the sample are assumed to follow the following relation (Arndt & Willis, 1966),

$$\beta(\mathbf{r}, \lambda) = (\lambda/\lambda')^4 \beta(\mathbf{r}, \lambda'), \quad (5)$$

$$\delta(\mathbf{r}, \lambda) = (\lambda/\lambda')^2 \delta(\mathbf{r}, \lambda'). \quad (6)$$

It may be noted that these relations hold good in the X-ray energy region where photoelectric effects dominate. Hence the following results may not be applicable where these relations do no not hold good. When the above conditions are satisfied, then the following relation between the absorption and phase at these two different wavelengths exists,

$$\varphi(\mathbf{r}, \lambda) = (\lambda/\lambda')\varphi(\mathbf{r}, \lambda'), \tag{7}$$

$$M(\mathbf{r}, \lambda) = (\lambda/\lambda')^3 M(\mathbf{r}, \lambda'). \tag{8}$$

Now consider equation (3). Let us assume the data have been collected at the wavelength λ_1, having phase φ_1 and absorption coefficient M_1,

$$\tilde{I}_{\lambda 1}(\mathbf{f}) = \tilde{\delta}(\mathbf{f}) + 2\sin(\pi\lambda_1 z|\mathbf{f}|^2)\widetilde{\varphi}_1(\mathbf{f}) - 2\cos(\pi\lambda_1 z|\mathbf{f}|^2)\widetilde{M}_1(\mathbf{f}). \tag{9}$$

Similarly let the data be collected at the wavelength λ_2, with phase shift φ_2 and absorption coefficient M_2,

$$\tilde{I}_{\lambda 2}(\mathbf{f}) = \tilde{\delta}(\mathbf{f}) + 2\sin(\pi\lambda_2 z|\mathbf{f}|^2)\widetilde{\varphi}_2(\mathbf{f}) - 2\cos(\pi\lambda_2 z|\mathbf{f}|^2)\widetilde{M}_2(\mathbf{f}). \tag{10}$$

By virtue of equations (7) and (8), equation (9) can be written in terms of the parameters $\widetilde{M}_1$ and $\widetilde{\varphi}_1$ as follows,

$$\tilde{I}_{\lambda 2}(\mathbf{f}) = \tilde{\delta}(\mathbf{f}) + 2\alpha\sin(\pi\lambda_2 z|\mathbf{f}|^2)\widetilde{\varphi}_1(\mathbf{f}) - 2\alpha^3\cos(\pi\lambda_2 z|\mathbf{f}|^2)\widetilde{M}_1(\mathbf{f}), \tag{11}$$

where $\alpha = (\lambda_2/\lambda_1)$. Thus there exists a definite relationship between the intensities at different wavelengths as defined by (11). Hence by collecting the data at different wavelengths one can again solve (3) by minimizing it with respect to the wavelength, *i.e.* $\min \sum_\lambda |2\alpha\sin(\pi\lambda z|\mathbf{f}|^2)\tilde{\varphi}(\mathbf{f}) - 2\alpha^3\cos(\pi\lambda z|\mathbf{f}|^2)\widetilde{M}(\mathbf{f}) - \tilde{I}_\lambda(\mathbf{f})|^2$ for the data collected at different wavelengths. This gives the following equation,

$$F(\varphi_1)(\mathbf{f}) = \frac{1}{2(B'C' - A'^2)}\Big[C'\sum_\lambda \tilde{I}_\lambda(\mathbf{f})\sin(\pi\lambda z|\mathbf{f}|^2)\alpha - A'\sum_\lambda \tilde{I}_\lambda(\mathbf{f})\cos(\pi\lambda z|\mathbf{f}|^2)\alpha^3\Big], \tag{12}$$

where

$$A' = \sum_\lambda \alpha^4 \sin(\pi\lambda z|\mathbf{f}|^2)\cos(\pi\lambda z|\mathbf{f}|^2),$$
$$B' = \sum_\lambda \alpha^2 \sin^2(\pi\lambda z|\mathbf{f}|^2),$$
$$C' = \sum_\lambda \alpha^6 \cos^2(\pi\lambda z|\mathbf{f}|^2).$$

This equation is very similar to equation (4) except for wavelength-dependent weight factors. This equation was used to retrieve the distribution of the projected phase map in the subsequent sections.

We have carried out some simulation studies to validate the correctness of this approach. A mathematical phantom as shown in Fig. 1(*a*) was simulated as an example of a weak phase object. The data were simulated to have a pixel pitch of 1 µm and 256 × 256 pixels were constructed. The maximum phase shift was restricted to [0, −1] rad for the simulated data. First we use equation (4) which relies on the variable-distance

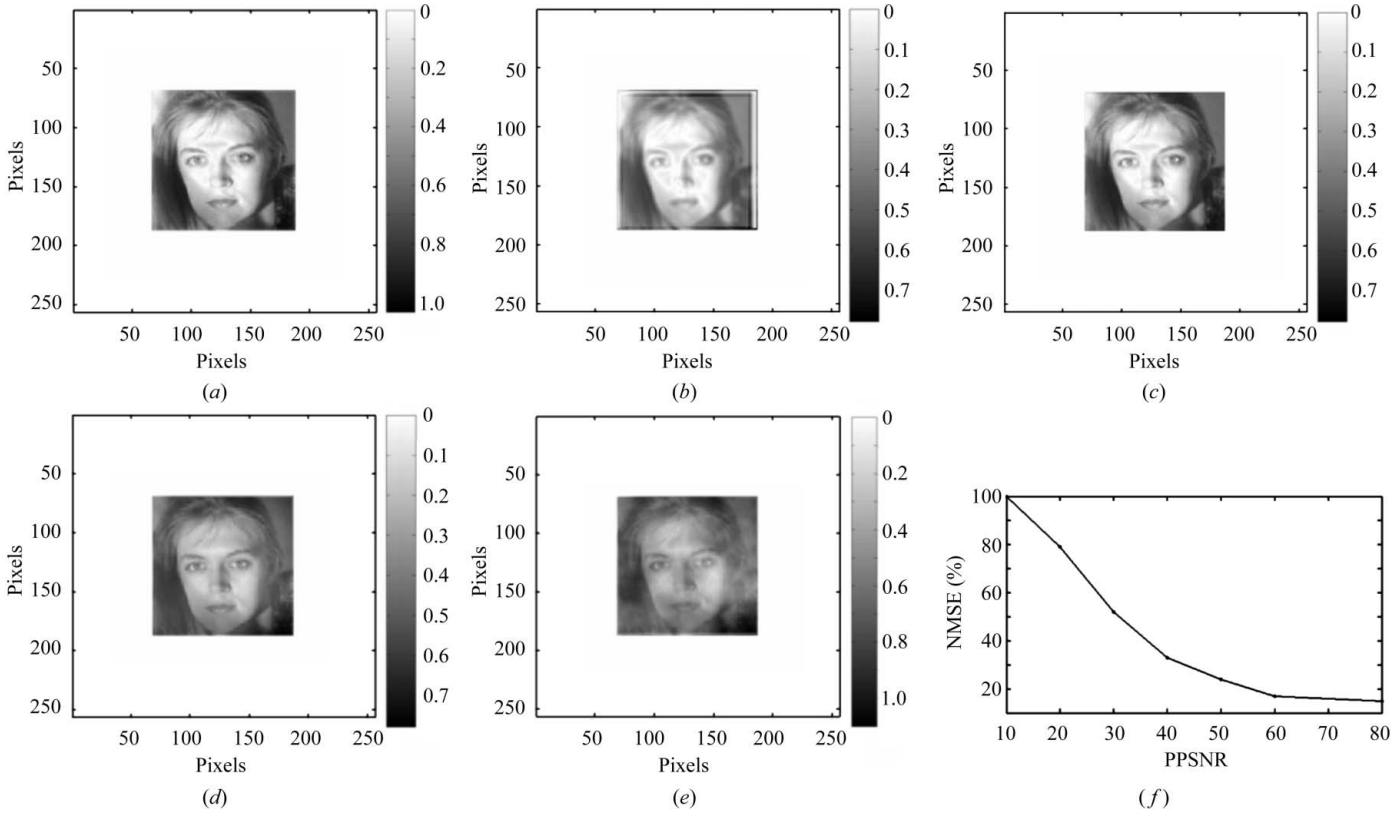

Figure 1
(*a*) Simulated phantom for illustration of the phase-retrieval approach. (*b*) Retrieved phase map using the variable-distance approach. (*c*) Retrieved phase map using the multi-wavelength approach. (*d*) Retrieved phase map using the multi-wavelength approach with 0.2% additive noise. (*e*) Retrieved phase map using the multi-wavelength approach with 0.5% additive noise. (*f*) Plot of normalized-mean square error (NMSE) (%) as a function of peak-to-peak signal-to-noise ratio (PPSNR) (dB).

approach for retrieving the phase from the simulated Fresnel diffraction. The Fresnel diffraction pattern was simulated [using equation (1)] for object-to-detector distances of 5 mm, 10 mm, 15 mm and 20 mm. Fig. 1(*b*) shows the retrieved phase map using the variable-distance approach. Fresnel diffraction at three different energies, $E = 16$ keV, 18 keV and 20 keV, was simulated and the phase map was retrieved using the variable-wavelength approach (Fig. 1*c*). It can be seen that the phase retrieved using the multi-wavelength approach is in agreement with the existing variable-distance approach.

We have also tested the phase-retrieval technique by adding white noise with zero mean to the simulated phase-contrast images. The simulations were repeated by adding 0.2% and 0.5% noise to the simulated phase-contrast images and then the multi-energy phase-retrieval method was applied. The results of the retrieved phase map are shown in Figs. 1(*d*) and Fig. 1(*e*). The technique of Tikhonov regularization (Tikhonov & Arsenin, 1977) was applied to these data so as to reduce the effect of noise. These results show that, in order to retrieve the phase map using this technique, very good signal-to-noise ratio is required. A plot of the normalized-mean square error (NMSE) (%) as a function of peak-to-peak signal-to-noise ratio (PPSNR) (dB) is shown in Fig. 1(*f*) to highlight the influence of noise in the reconstruction process

4. Experimental results

We have used the SYRMEP beamline at Synchrotron Trieste (Italy) (Nugent *et al.*, 1996) for these studies. This is a third-generation synchrotron facility, which can run at 2.0 or 2.4 GeV with a maximum ring current of 320 or 140 mA, respectively. The cross-sectional dimensions of the electron bunches circulating in the storage ring are approximately 1100 × 140 μm (full width at half-maximum). A monolithic channel-cut Si (111) crystal is used to choose the monochromatic X-rays from the incoming white beam. A monochromatic beam, within the energy range 8–35 keV and an energy resolution of about 0.2%, is thus available in the experimental area. The beamline is characterized by a large source-to-sample distance of 22 m, a monochromatic laminar-section X-ray beam with a maximum area of 120 × 4 mm. The provision to vary sample-to-detector distances up to 1.8 m is available for the in-line phase-contrast imaging experiments. A CCD detector and fiber-optic combination having an effective pixel pitch of 4. μm were used for collecting high-resolution phase-contrast images.

Silicon aerogel was chosen as a low-absorption sample for application of the multi-wavelength formulation. Silicon aerogel with fibrous structure was prepared to study the wavelength-based approach for phase retrieval. These aerogels have some very interesting properties such as low density, high strength, *etc.* They are used to produce clean fuels, to insulate windows and even clothing, to study the percolation of oil through rock, and as drug-delivery systems. Fig. 2 shows a phase radiograph of the sample at different energies. The object-to-detector distance was kept at $z = 50$ cm. It can be seen from Figs. 2(*a*)–2(*c*) that, as the energy of the X-ray

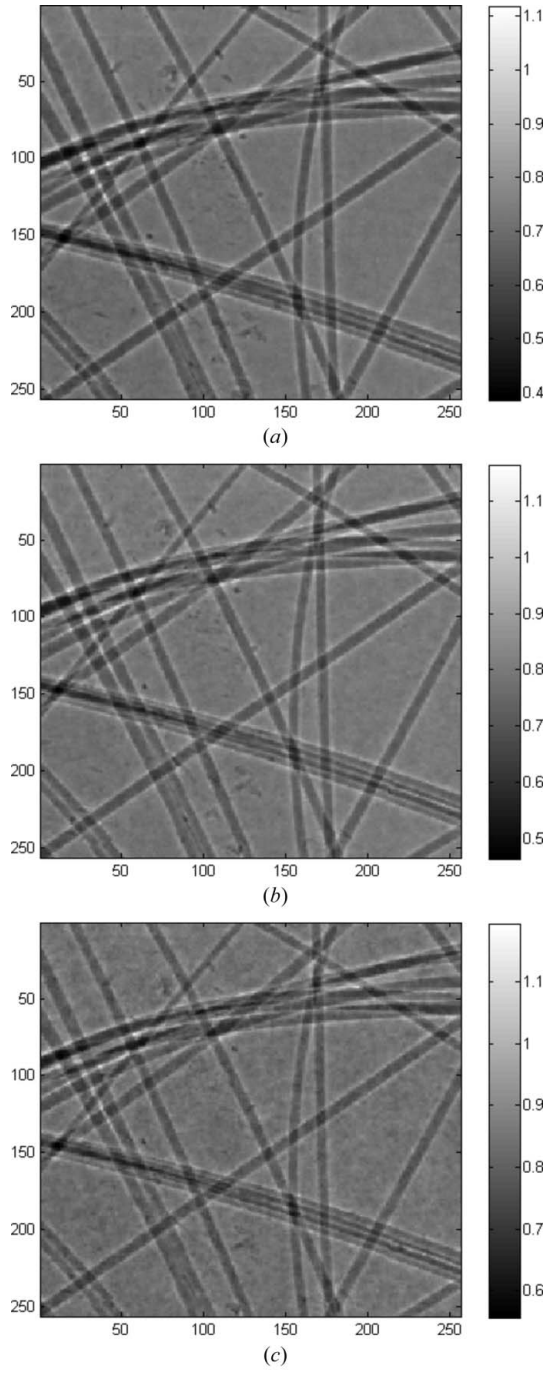

Figure 2
Phase radiographs of the fibrous structure within silicon aerogel at $E =$ (*a*) 16 keV, (*b*) 18 keV and (*c*) 20 keV.

increases, the edge contrast decreases. This is in accordance with the fact that the phase shift decreases with increase in energy. Moreover, even with the flat-field correction, the effect of an inhomogeneous background owing to a beryllium window was not properly corrected. The noticeable variation in background across the image can be seen in these phase radiographs.

The phase radiographs at three different energies ($E =$ 16 keV, 18 keV and 20 keV) were used as input to equation (12). The retrieved projected phase profile is shown in Fig. 3.

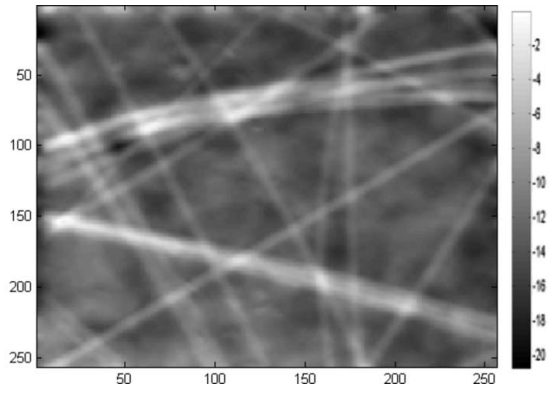

Figure 3
Retrieved phase map of the fibrous structure of silicon aerogel using the multi-wavelength approach.

As reported in the simulation, the quality of reconstruction critically depends upon the signal-to-noise ratio. In this experiment we could not properly remove the effect of inhomogeneous absorption of the beryllium window, thereby achieving a poor signal-to-noise ratio, which resulted in an inhomogeneous variation of the background in the reconstructed image. However, the major features such as fiber structures can be easily recognized and located. This experiment shows that within the framework of the CTF-based approach one can retrieve the projected phase map using the multi-wavelength-based formulation. This method can be used as an alternative approach to the existing method of phase retrievals when variations with respect to different distances are difficult to perform, owing to constraints of the experimental set-up, and retrieval of the phase information is important.

5. Conclusion

We have proposed a variable-wavelength-based phase-contrast approach for retrieving the phase of weakly absorbing objects using a CTF-based formulation. This approach helps to eliminate any motion of the sample, thereby eliminating any misalignment during data collection, and thus making it more computationally efficient. This approach may also be useful in phase retrieval using other sources of radiation where the option of change of the wavelength of radiation exists.

This work was carried out under ICTP-ELETTRA (Trieste) proposal No. 2006667 at the SYRMEP beamline. The authors are grateful to Giuliana Tromba, Fulvia Arfelli, Luigi Rigon and Diego Dreossi for their help during the experiment.

References

Allen, L. J. & Oxley, M. P. (2001). *Opt. Commun.* **199**, 65–75.
Arndt, U. W. & Willis, B. T. M. (1966). *Single Crystal Diffractometry*, p. 185. Cambridge University Press.
Barty, A., Nugent, K. A., Paganin, D. & Roberts, A. (1998). *Opt. Lett.* **23**, 817–819.
Bonse, U. & Hart, M. (1965). *Appl. Phys. Lett.* **6**, 155–156.
Bronnikov, A. V. (2002). *J. Opt. Soc. Am. A*, **19**, 472–480.
Chapman, D., Thomlinson, W., Johnston, R. E., Washburn, D., Pisano, E., Gmür, N., Zhong, Z., Menk, R., Arfelli, F. & Sayers, D. (1997). *Phys. Med. Biol.* **42**, 2015–2025.
Cloetens, P., Barrett, R., Baruchel, J., Guigay, J. P. & Schlenker, M. (1996). *J. Phys. D*, **29**, 133–146.
Cloetens, P., Ludwig, W., Baruchel, J., Dyck, D. V., Landuyt, J. V., Guigay, J. P. & Schlenker, M. (1999). *Appl. Phys. Lett.* **75**, 2912–2914.
David, C. Nöhammer, B. Solak, H. H. & Ziegler, E. (2002). *Appl. Phys. Lett.* **81**, 3287–3289.
Groso, A., Abela, R. & Stampanoni, M. (2006). *Opt. Express*, **14**, 8103–8110.
Guigay, J. P. (1977). *Optik*, **46**, 121–125
Guigay, J. P., Langer, M., Boistel, R. & Cloetens, P. (2007). *Opt. Lett.* **32**, 1617–1619.
Gureyev, T. E., Mayo, S., Wilkins, S. W., Paganin, D. M. & Stevenson, A. W. (2001). *Phys. Rev. Lett.* **86**, 5827–5830.
Gureyev, T. E. & Nugent, K. A. (1997). *Opt. Commun.* **133**, 339–346.
Gureyev, T. E., Paganin, D., Stevenson, A. W., Mayo, S. & Wilkins, S. W. (2004). *Phy. Rev. Lett.* **93**, 068103.
Gureyev, T. E., Pogany, A., Paganin, D. M. & Wilkins, S. W. (2004). *Opt. Commun.* **231**, 53–70.
Gureyev, T. E., Stevenson, A. W., Paganin, D. M., Weitkamp, T., Snigirev, A., Snigireva, I. & Wilkins, S. W. (2002). *J. Synchrotron Rad.* **9**, 148–153.
Langer, M., Peyrin, P. F., Cloetens, P. & Guigay, J. (2008). *Med. Phys.* **35**, 4556–4566.
Meng, F., Liu, H. & Wu, X. (2007). *Opt. Express*, **15**, 8383–8390.
Momose, A. (2003). *Opt. Express*, **11**, 1303–1314.
Nugent, K., Gureyev, T., Cookson, D., Paganin, D. & Barnea, Z. (1996). *Phys. Rev. Lett.* **77**, 2961–2964.
Paganin, D. & Nugent, K. A. (1998). *Phys. Rev. Lett.* **80**, 2586–2589.
Pfeiffer, F., Weitkamp, T., Bunk, O. & David, C. (2006). *Nat. Phys.* **2**, 258–261.
Snigirev, A., Snigireva, I., Kohn, V., Kuznetsov, S. & Schelokov, I. (1995). *Rev. Sci. Instrum.* **66**, 5486
Teague, M. R. (1982). *J. Opt. Soc. Am.* **72**, 1199–1209.
Teague, M. R. (1983). *J. Opt. Soc. Am.* **73**, 1434–1441.
Tikhonov, A. N. & Arsenin, V. A. (1977). *Solution of Ill-Posed Problems.* New York: Winston & Sons.
Turner, L. D., Dhal, B. B., Hayes, J. P., Nugent, K. A., Paterson, D., Scholten, R. E., Tran, C. Q. & Peele, A. G. (2004). *Opt. Express*, **12**, 2916.
Wilkins, S. W., Gureyev, T. E., Gao, D., Pogany, A. & Stevenson, A. W. (1996). *Nature (London)*, **384**, 335–338.
Zabler, S., Cloetens, P., Guigay, J.-P., Baruchel, J. & Schlenker, M. (2005). *Rev. Sci. Instrum.* **76**, 1–7